The Reflection of a Stationary Gravity Wave by a Viscous Boundary Layer

François Lott
Laboratoire de Météorologie Dynamique du CNRS,
Ecole Normale Supérieure,
24, rue Lhomond, 75231 PARIS cedex 05, France

Revised version: December 18, 2006

Abstract

The backward reflection of a stationary Gravity Wave (GW) propagating toward the ground is examined in the linear viscous case and for large Reynolds numbers ($\mathcal{R}e$). In this case, the stationary GW presents a critical level at the ground because the mean wind is null there. When the mean flow Richardson number at the surface (J) is below 0.25, the GW reflection by the viscous boundary layer is total in the inviscid limit $\mathcal{R}e \to \infty$. The GW is a little absorbed, when $\mathcal{R}e$ is finite, and the reflection decreases when both the dissipation and J increase. When $J > 0.25$, the GW is absorbed for all values of the Reynolds number, with a general tendency for the GW reflection to decrease when J increases. As a large ground reflection favors the downstream development of trapped lee wave, the fact that it decreases when J increases explains why the more unstable boundary layers favor the onset of mountain lee waves. It is also shown that the GW reflection when $J > 0.25$ is substantially larger than that predicted by the conventional inviscid critical level theory, and than that predicted when the dissipations are represented by Rayleigh friction and Newtonian cooling.

The fact that the GW reflection depends strongly on the Richardson number indicates that there are some correspondences between the dynamics of trapped lee-waves and the dynamics of Kelvin-Helmholtz instabilities. Accordingly, and on one classical example, it is shown that some among the neutral modes for Kelvin-Helmholtz instabilities that exist in an unbounded flow when $J < 0.25$, can also be stationnary trapped-wave solutions in the presence of a ground and in the inviscid limit $\mathcal{R}e \to \infty$. When $\mathcal{R}e$ is finite, these solutions are affected by the dissipation in the boundary layer and decay in the downstream direction. Interestingly, their decay rate increases when both the dissipation and J increase, as does the GW absorption by the viscous boundary layer.

1 Introduction

The conventional linear theory of trapped lee waves assumes that mountains excite free modes of oscillations (Scorer 1949). These modes are constituted of stationary gravity waves which are entirely reflected downward at a turning altitude located in the mid-troposphere and entirely reflected upward at the ground. Although this theory is largely supported by observations, there are situations where the atmospheric conditions aloft are favorable for the low-level trapping of

gravity waves but where lee waves are not observed (Smith et al. 2002). A plausible explanation is that the GWs are absorbed in the boundary layer (Smith et al. 2006). This process can be very efficient because the wind at the ground is null, so that stationary gravity waves have a critical level there (Jiang et al. 2006). If the GWs-critical level interaction theory applies in this case (Booker and Bretherton 1967, hereinafter BB67) it predicts that the GWs can be very efficiently absorbed if the Richardson number of the background flow at the ground, J, is larger than 0.25.

Over the last 20 years, numerical simulations have established that the mesoscale mountain flow dynamics is substantially affected by the presence of a boundary layer (Bougeault and Lacarrere 1989, Richard et al 1989, Georgelin et al 1994). In these papers, it is shown that the specification of the surface friction and the treatment of the turbulent dissipation in the boundary layer parameterization schemes affect the onset of the downslope windstorms and the development of mountain waves. The tuning of these parameters was a prerequisite to reproduce the flow observed during the PYREX experiment (Bougeault et al. 1991). More recently, Smith et al. (2002) have shown that the impact of the boundary layer can become extremely strong, in particular when the low-level air between the mountain peaks is stagnant. They have shown, interpreting data from the MAP experiment (Bougeault et al. 2001), that the stagnant layer can absorb the downward propagating waves and inhibit the development of trapped lee waves. It is in this context that they have introduced the concept of a reflective factor of the stationnary wave by the boundary layer q: when the amplitude of this factor is near $|q| = 1$ the downward stationnary gravity wave is almost entirely reflected, and trapped lee-waves develop over a long distance downstream of the mountain. When $|q|$ is small, the downward wave is absorbed and the trapped lee-waves rapidly decay downstream. This factor also turns out to be efficient in explaining the downstream development of trapped lee waves in a quite extensive set of mesoscale simulations (Jiang et al. 2006). More recently, Smith et al. (2006) simplified the boundary layer dynamics to bulk formula for the stresses at the boundary layer interfaces, and showed that the frictional forces at the top and at the bottom of the boundary layer can shift upstream the disturbance in the boundary layer. This configuration yields to an energy loss which explains the absorption of the disturbance by the boundary layer.

It is quite clear that these papers deepens our understanding of the trapped lee-waves dynamics. The dynamical interpretation they provide are nevertheless based on highly simplified mathematical models: in Jiang et al. (2006) the frictions are represented by linear dampings, in Smith et al. (2006), they are represented by bulk formula for stresses that are applied at the interfaces of the boundary layer only. Accordingly, it seems worthwhile to evaluate q in the case of a stably stratified viscous boundary layer and for smooth background profiles. The central reason for choosing this particular set-up is that the physics and the dynamics of a viscous and thermally conducting fluid are not controlled by arbitrary tuning parameters and are very comprehensive. It also permits to treat analytically and in a continuous way the transition from the boundary layer to the free atmosphere. Nevertheless, in this set-up, the GW absorptions due to a stagnant or to a convectively well mixed boundary layer are neglected. Still in this set-up, the influence on the GW absorption of the partial reflections occurring at the top of the boundary layer where the wind and stratification vary abruptly are also neglected.

Although the interaction between GWs and critical levels has been the subject of many papers during the last 40 years (see references in Lott and Teitelbaum, 1993), little attention has been given to the rather peculiar circumstance where the critical level is exactly located on a rigid surface. In this case, it is not obvious that the GW really feels the influence of the critical level, and that the behavior of the solution remains very sensitive to the value of J.

If it is the case, the sensitivity of the trapped lee waves dynamics to the value of J, and the fact that the critical level dynamics plays a significant role, also suggest that there are some correspondences between trapped lee waves and Kelvin-Helmholtz instabilities.

To emphasize that the problem needs dissipation, it is important to recall that the inviscid problem is rather degenerated in the stationary case. In this case, BB67 have shown that the disturbance near the ground is the combination of two independent solutions which vertical velocity tends toward 0 when once approaches a critical level (see their Eq. 2.5). They both satisfy the inviscid boundary condition $w = 0$ when the critical level is at the ground. This leaves undetermined the evaluation of the fraction between the two, and it is this fraction which ultimately controls the disturbance absorption by the critical level.

The first purpose of this note is to evaluate the fraction between the two inviscid solutions of BB67 when the critical level is at the ground and by adding a small dissipation. The case where the dissipation is due to viscosity and thermal diffusivity is detailed. The case where it is due to Rayleigh friction and Newtonian cooling is briefly discussed. The second is to use this result to evaluate the reflection q of a GW coming from $z \to \infty$. The third is to illustrate that there are correspondences between trapped lee-waves and the Kelvin-Helmholtz instabilities.

The plan of this note is as follows. Section 2 gives the basic equations and recalls some properties of the two independent inviscid solutions of BB67. The viscous solutions in the viscous boundary layer are evaluated in Section 3 and matched with these two inviscid solutions. Section 4 translates this result in terms of the reflection of a GW coming from $z = \infty$. It also translates it in terms of trapped waves solutions. For these purposes, the classical mean flow profile used by Van Duin and Kelder (1982) to study the absorption of a GW by a critical level and by Drazin (1958) to study Kelvin-Helmholtz instabilities is adopted in Section 4. Section 5 discusses the results obtained in relation with our current knowledge of the GWs-critical level dynamics. Their significance for the theory of trapped lee-waves is also presented. Appendix A treats the case where the dissipations are due to Rayleigh friction and Newtonian cooling.

2 Basic equations and inviscid solution near the ground

2.1 Physical set-up and background flow definition

The fluid considered is non-rotating, viscous, and thermally conducting. Its kinematic viscosity ν and its thermal conductivity κ are both constant. In the absence of perturbations, this fluid has a velocity $U(z)$ oriented along the horizontal x-axis, varying in the vertical direction z and null at the ground (e.g. in $z = 0$). Its characteristic amplitude outside of the shear layer is U_0 and the length scale representative of the shear layer depth is $D = U_0/U_z(0)$. Here the z subscript is for the vertical derivation. The fluid is also stratified with an undisturbed density $\rho_0(z)$ decreasing with altitude so that the Brunt-Vaisala frequency $N^2 = -\frac{g}{\rho_0(0)}\frac{d\rho_0}{dz}$ is positive. Here g is the gravitational acceleration and ρ_r is a reference constant. The Boussinesq approximation is adopted, we will note N_0^2 the value of N^2 at the ground, and take $\rho_0(0) = \rho_r$.

Although the more general results presented are related to the dynamics of the GWs inside and just above the viscous boundary layer, their consequences in the far field will be illustrated for mean flow profiles that vary like,

$$U(z) = U_0 \tanh(z/D), \; N^2 = N_0^2, \tag{1}$$

e.g. that present a smooth transition from the region near the ground where the wind shear is almost constant ($z << D$) to large altitudes where the wind is almost constant ($z >> D$).

It is important to note that the background density profile yielding to N^2 in Eq. 1 varies linearly in z, so that it is an exact solution of the diffusion equation (e.g. because $\rho_{0zz} = 0$). This is not strictly true for the wind profile $U(z)$, but the error is rather small everywhere at large Reynolds number. More significantly, $U(z)$ is almost an exact solution of the viscous equation near the ground, because it almost varies linearly with z when $z << D$ (again because $U_{zz} \approx 0$ there).

The stationary perturbations analyzed have a dependence in x of the form $\exp(ikx)$ where k is a real horizontal wavenumber. Introducing U_0, $D = U_0/U_z(0)$, $\rho_r U_0^2$, $\rho_r U_0^2/(gD)$ as scales for the velocities, the length, the perturbation of pressure and the perturbation of density respectively, the dimensionless form of the equations for the perturbation are:

$$ikUu + U_z w + ikp = \mathcal{R}e^{-1}\left(u_{zz} - k^2 u\right), \quad ikUw + p_z + \rho = \mathcal{R}e^{-1}\left(w_{zz} - k^2 w\right),$$
$$iku + w_z = 0, \quad ikU\rho - JN^2 w = (\mathcal{P}r\mathcal{R}e)^{-1}\left(\rho_{zz} - k^2\rho\right). \tag{2}$$

In Eqs. 2, u, w, p, and ρ are complex dimensionless functions, representing the perturbations of horizontal wind, vertical wind, pressure, and density respectively. Still in Eq. 2,

$$\mathcal{R}e = \frac{U_0 D}{\nu}, \ \mathcal{P}r = \frac{\kappa}{\nu}, \text{ and } J = \frac{N_0^2 D^2}{U_0^2}, \tag{3}$$

are the Reynolds number, the Prandtl number and the Richardson number at the ground respectively. Note also that in Eqs. 2 and from now, z, k, $U(z)$ and $N(z)$ are also dimensionless. For this set of equations the boundary conditions at the ground are:

$$u(0) = \rho(0) = w(0) = 0. \tag{4}$$

2.2 Inviscid solutions

When the Reynolds number is large, the solution is very well approximated by its inviscid solution, e.g. by the solution of Eqs. 2 with all terms on the right hand sides put to zero. In this limit, Eqs. 2 reduce to the Taylor-Goldstein equation:

$$w_{zz} + \left(\frac{JN^2}{U^2} - \frac{U_{zz}}{U} - k^2\right) w = 0. \tag{5}$$

For small z, BB67 have derived the leading order behavior of the solution near $z = 0$. When $J > 0.25$ it is given by

$$w \approx Az^{1/2+i\mu} + Bz^{1/2-i\mu}, \quad \text{where } \mu = \sqrt{|J - 1/4|}, \tag{6}$$

and where A and B are two complex constants. When $J < 0.25$ the same equation applies by changing μ in $i\mu$.

When $J > 1/4$, the momentum flux associated with the inviscid solution in Eq. 6 is given by

$$\frac{uw^* + u^* w}{4} = -\frac{\mu}{2k}\left(|A|^2 - |B|^2\right) = +\frac{\mu|B|^2}{2k}\left(1 - |R|^2\right), \tag{7}$$

where the $*$ is for the complex conjugate, and R is the fraction between the two solutions of BB67:

$$R = A/B. \tag{8}$$

When $J < 1/4$ the momentum flux near $z = 0$ is given by

$$\frac{uw^* + u^* w}{4} = \frac{i\mu}{2k}\left(A^* B - B^* A\right) = +\frac{\mu|B|^2}{k}|R|\sin\phi, \tag{9}$$

where ϕ is the phase of R: $R = |R| \exp i\phi$.

It is noteworthy that the inviscid solution in Eq. 6 satisfies the inviscid boundary condition $w(0) = 0$ for all values of A and B and does not permit to evaluate R: near the ground, it is necessary to solve the viscous Equations and to match the result to the inviscid solution.

3 Solution in the viscous layer and matching

3.1 Method

To evaluate the viscous solutions near the ground, the Eqs. 2 are rescaled using the inner vertical coordinate and the inner variables (Hazel 1967):

$$z = \delta\tilde{z},\ w = k\delta\tilde{w},\ u = \tilde{u},\ p = \delta\tilde{p},\ \rho = \tilde{\rho},\ \text{and where } \delta = (k\mathcal{R}e)^{-1/3}\,. \tag{10}$$

Here, δ characterizes the depth over which the viscous effects are important. In the limit of small δ the set of Eqs. (2) is well approximated by:

$$i\tilde{z}\tilde{u} + \tilde{w} + i\tilde{p} = \tilde{u}_{\tilde{z}\tilde{z}},\ \ \tilde{p}_{\tilde{z}} + \tilde{\rho} = 0,\ \ i\tilde{u} + \tilde{w}_{\tilde{z}} = 0,\ \ i\tilde{z}\tilde{\rho} - J\tilde{w} = \mathcal{P}r^{-1}\tilde{\rho}_{\tilde{z}\tilde{z}}\,. \tag{11}$$

This set of Equations admits six independent solutions, their asymptotic form for $\tilde{z} \to \infty$ can be found in Baldwin and Roberts (1970). When $J > 0.25$ they are given by:

$$\begin{aligned} &\tilde{w}_1 \sim \tilde{z}^{1/2+i\mu}, \qquad \tilde{w}_2 \sim \tilde{z}^{1/2-i\mu}, \qquad \tilde{w}_3 \sim \tilde{z}^{-5/4}e^{-\frac{2}{3}\sqrt{i}\tilde{z}^{3/2}}, \\ &\tilde{w}_4 \sim \tilde{z}^{-9/4}e^{-\frac{2}{3}\sqrt{i\mathcal{P}r}\tilde{z}^{3/2}}, \quad \tilde{w}_5 \sim \tilde{z}^{-5/4}e^{+\frac{2}{3}\sqrt{i}\tilde{z}^{3/2}}, \quad \tilde{w}_6 \sim \tilde{z}^{-9/4}e^{+\frac{2}{3}\sqrt{i\mathcal{P}r}\tilde{z}^{3/2}}. \end{aligned} \tag{12}$$

Because the solutions $\tilde{w}_5$ and $\tilde{w}_6$ tend exponentially toward ∞ when $\tilde{z} \to \infty$ they cannot match the inviscid solution when $\tilde{z} \to \infty$ (Van Duin and Kelder 1986), so they have to be dropped from the inner solution:

$$\tilde{w} = \tilde{A}\tilde{w}_1 + \tilde{B}\tilde{w}_2 + \tilde{C}\tilde{w}_3 + \tilde{D}\tilde{w}_4. \tag{13}$$

To evaluate the 4 viscous solutions ($\tilde{w}_i, i = 1, 4$), the Eqs. 11 are integrated downward numerically using the Brankin et al. (1991) Runge-Kutta library subroutine. The integration starts at the altitude $\tilde{z} = 5$ and finishes at $\tilde{z} = 0$ (see also Hazel 1967). For each solution, the starting values for $\tilde{w}_i$ and its first five derivatives are deduced from Eqs. 12. For each solution, the ground values $\tilde{w}_i(0)$, $\tilde{u}_i(0)$, and $\tilde{\rho}_i(0)$ combined with the three boundary conditions (Eq. 4) permit to evaluate $\tilde{A}$, $\tilde{C}$ and $\tilde{D}$ as a function of $\tilde{B}$. Following Van Duin and Kelder (1986), this solution is then matched to the inviscid solution in (6) by taking:

$$A = \tilde{A}k\delta^{1/2-i\mu},\ B = \tilde{B}k\delta^{1/2+i\mu}. \tag{14}$$

This matching can also be written

$$R = \delta^{-2i\mu}\tilde{R}\ \ \text{, where}\ \ \tilde{R} = +\tilde{A}/\tilde{B} \tag{15}$$

is the "inner" coefficient measuring the fraction between the two viscous solutions that match the inviscid solution in Eq. 6.

3.2 Results

The results of two numerical integrations are presented in Figs. 1a) and 1b) for $J = 0.1$ and $J = 0.5$, respectively (for the other parameters, see the Fig. 1 caption). In these integrations $\tilde{B}$ is fixed, the inner solution is evaluated as described in the Section 3.1 giving $\tilde{A}$, and the matching conditions in Eq. 14 give A and B. The inviscid solution is then evaluated using Eq. 6. To check that the viscous and the non-viscous solution recover each other over a large zone, the viscous equations are also integrated up to $\tilde{z} = 10$ and the inviscid solution is displayed down to $\tilde{z} = 1$.

The amplitude of $\tilde{u}$, $\tilde{w}$, and $\tilde{\rho}$ are shown as a function of the inner vertical coordinate $\tilde{z}$ in Figs. 1a, b (left panels). Also shown are the corresponding inviscid solutions expressed with the inner variables u, $w/(k\delta)$ and ρ (dashed lines). For these three variables, there is a smooth transition from the full viscous solution to the inviscid one when $1 < \tilde{z} < 5$. Note as well that the full viscous solutions and the inviscid solutions are almost equal everywhere between $\tilde{z} = 5$ and $\tilde{z} = 10$. It is also interesting to note that the phase of all the variables decreases with

altitude in both cases considered in Figs. 1a, b (right panels). It means that the perturbations in the viscous layer are shifted upstream when compared to the phase of the disturbances above the viscous layer. As shown by Smith et al. (2006) in an other simple model of the boundary layer, this phase shift is the fundamental cause of the absorption by the boundary layer.

To quantify more precisely this absorption, the Fig. 2 gives the value of the coefficient $\tilde{R}$ and for few Prandtl numbers $0.2 < \mathcal{P}r < 5$. When $J < 0.25$, the amplitude $|\tilde{R}|$ is always larger than 0.75, it increases monotonically when J increases and becomes equal to 1 exactly when $J = 0.25$. When $J > 0.25$, $|\tilde{R}|$ decreases as J increases, going to zero as $J \to \infty$. Note that the amplitude $|\tilde{R}|$ in Fig. 2 is almost insensitive to the value of the Prandtl number $\mathcal{P}r$, at least in the domain considered ($0.2 < \mathcal{P}r < 5$). The dashed lines in Fig. 2 are for the phase $\tilde{\phi}$. When $J < 0.25$ it is positive and slightly smaller than π, its value is insensitive to the value of the Prandtl number. When $J > 0.25$, $\tilde{\phi}$ can take all values between $-\pi$ and $+\pi$, it also becomes sensitive to the value of the Prandtl number.

For the inviscid fraction R, its relationships with $\tilde{R}$ in Eq. 15 makes that its amplitude $|R| = |\tilde{R}|$ when $J > 1/4$. This allows to rewrite the momentum flux expression in Eq. 7:

$$\frac{uw^* + u^*w}{4} = +\frac{\mu|B|^2}{2k}\left(1 - |\tilde{R}|^2\right) > 0. \tag{16}$$

It is positive because $|\tilde{R}| < 1$ when $J > 1/4$ (Fig. 2). As a positive momentum flux corresponds to a downward propagating disturbance, Eq. 16 proves that there is absorption by the viscous layer. Note also that the momentum flux in Eq. 16 is indicative that the absorption increases when J increases, because $|\tilde{R}|$ decreases toward 0 in this case (Fig. 2).

When $J < 1/4$, the matching in Eq. 15 still applies by changing μ in $i\mu$ so the momentum flux in Eq. 9 can be written:

$$\frac{uw^* + u^*w}{4} = \delta^{2\mu}\frac{\mu|B|^2}{k}|\tilde{R}|\sin\tilde{\phi} > 0. \tag{17}$$

It is again positive, but in this case this is due to the fact that the phase $0 < \tilde{\phi} < \pi$ (Fig. 2). The stationary disturbance is again absorbed by the viscous layer. Note that in this case, the presence of the very small term $\delta^{2\mu}$ in Eq. 17 indicates that the absorption is small when $J < 1/4$. In particular, in the infinite Reynolds number limit, $\delta \to 0$, and the momentum flux in Eq. 17 becomes null: the GW is entirely reflected by the ground.

4 Application to a varying background shear

At this stage, to quantify even more precisely the absorption, it is important to recall that it is not trivial to relate the solutions of BB67 to upward propagating waves in $z = \infty$. In other words, the coefficient B in Eqs. 16–17 is not measuring the amplitude of a GW propagating toward the surface (except in the WKB limit $J >> 1$ see BB67). To circumvent this difficulty, we next adopt the mean flow profiles in Eq. 1. For these profiles, exact inviscid solutions to the Taylor-Goldstein equation (Eq. 5) exist (see VK82 or Lott et al. 1992 for details), when $J > 0.25$ and $J > k^2$ they are given by

$$w = A\, r^{1/4+i\mu/2}(1-r)^{-im/2}F\left(\frac{5}{4} + i\frac{\mu}{2} - i\frac{m}{2}, -\frac{1}{4} + i\frac{\mu}{2} - i\frac{m}{2}; 1 + i\mu; r\right)$$
$$+B\, r^{1/4-i\mu/2}(1-r)^{-im/2}F\left(\frac{5}{4} - i\frac{\mu}{2} - i\frac{m}{2}, -\frac{1}{4} - i\frac{\mu}{2} - i\frac{m}{2}; 1 - i\mu; r\right), \tag{18}$$

where F is the Hypergeometric function, $r = \tanh^2 z$, and $m = \sqrt{|J - k^2|}$ is the vertical wavenumber of the disturbance in $z \to \infty$. Note that the k^2 part of m is a non-hydrostatic term and that the coefficients A and B in Eq. 18 are the same as in Eq. 6 (in particular because $F(.,.;.;0) = 1$). Note also that Eq. 18 still applies when $J < 1/4$ or/and when $J < k^2$ by changing μ in $i\mu$ or/and m in im. To describe the solution in $z \to \infty$ the following linear transformation formula for F can be used (see for instance Oberhettinger 1970):

$$\begin{aligned} F(a,b;c;r) = & \quad \tfrac{\Gamma(c)\Gamma(c-a-b)}{\Gamma(c-a)\Gamma(c-b)} F(a,b;a+b-c+1,1-r) \\ +(1-r)^{c-a-b} & \quad \tfrac{\Gamma(c)\Gamma(a+b-c)}{\Gamma(a)\Gamma(b)} F(c-a,c-b;c-a-b+1;1-r), \end{aligned} \tag{19}$$

where Γ is the Gamma function, while a, b and c are complex constants. The use of this transformation (19) in the solution (18) permits to shows that in $z \to \infty$

$$w \approx U_p \, e^{+imz} - D_o \, e^{-imz}. \tag{20}$$

Here the sign convention is as in Jiang et al. (2006), while U_p and D_o are linear combinations of A and B with coefficients given by products and fractions of Gamma functions.

4.1 Propagating solutions: $J > k^2$

When $J > k^2$ the first solution in Eq. 20 is an upward propagating GW and the second a downward propagating GW. Hence the reflection coefficient is

$$q = U_p / D_o. \tag{21}$$

Its amplitude $|q|$ is shown in Fig. 3 and for a wavenumber $k = 10^{-1}$, which ensures vertical wave propagation in $z \to \infty$ for all values of $J > 10^{-2}$.

As expected from the results in Section 3, the incident wave D_o is almost entirely reflected ($|q| = 1$) when $J < 0.25$, at least when δ is below 10^{-4} (thin solid lines corresponding to $\delta = 10^{-8}$ and $\delta = 10^{-4}$ in Fig. 3). Some absorption occurs when δ increases, but it is small (thin solid line corresponding to $\delta = 10^{-2}$).

When $J > 0.25$, and for the three values of δ shown (thin lines in Fig. 3) the amplitude of the reflection factor $|q|$ is below 1. In this case and for a fixed δ, the values for $|q|$ vary around $|\tilde{R}|$ when J increases. More precisely, $|q|$ presents a series of local minima and maxima which converge toward $|\tilde{R}|$ when J increases. The presence of these extrema is related to the fact that the matching condition in Eq. 15 affects the phase of the fraction between the two inviscid solutions of BB67 (R): when J increases, the relative phase of the coefficient $\delta^{i\mu}$ that links R and $\tilde{R}$ in Eq. 15 varies much more over the same range of μ when δ is small than when it is large. This explains the larger number of extrema for $|q|$ when δ is small. Note also that the number of extrema when $\delta = 10^{-2}$ is already quite small, which means that this effect should not be very pronounced for the real atmospheric boundary layer.

To provide upper and lower bounds for $|q|$ that take into account this effect, the thick solid line and the dotted line in Fig. 3 show the maximum values and the minimum values of $|q|$ when δ varies and when J is fixed. These curves show that $|q|$ is always below 1 and never 20% larger than $|\tilde{R}|$, but can be can be substantially smaller than $|\tilde{R}|$. Nevertheless, when $J > 2$ the two curves almost coincide, making of the inner fraction $|\tilde{R}|$ a good estimate of the GW reflection $|q|$. Overall, the monotonic decay of the upper and lower bounds for $|q|$ when J increases prove that there is a general tendency for the GW absorption to increase when J increases.

It is important to note that the boundary layer Reflection of the incident wave is very different from the reflection due to a full critical level interaction (e.g. when there is no rigid boundary, see the thick grey dashed line in Fig. 3). On the one hand, when $J < 0.25$ the

boundary layer reflection is very near 1 while in the case of a full critical level interaction it can becomes very large when $J \to 0$. On the other hand, when $J > 0.25$, the boundary layer reflection is substantially larger than the full critical level reflection. Note that when the dissipations are due to Newtonian cooling and Rayleigh friction, the reflection is near 1 when $J < 0.25$, as in the viscous case, but is substantially smaller than the viscous boundary layer reflection when $J > 0.25$ (see Appendix). This shows that the use of linear dampings can lead to overestimate the GW absorption near the surface.

4.2 Evanescent solutions: $J < k^2$

When $J < k^2$, m is changed in im in Eq. 20, so the first term in the left hand side of Eq. 20 is a disturbance that decays exponentially with altitude, the second becomes infinite when $z \to \infty$. Accordingly, the only acceptable solutions are those for which $D_o = 0$ in Eq. 20: the disturbance is not excited by an incident wave coming from ∞, it is a free mode of oscillation.

To find these solutions, it is essential to recall that for the profiles in Eq. 1 and for an unbounded domain, the neutral modes of the Taylor-Goldstein Equation (Eq. 5) are known (Drazin 1958), and only exist when $J < 0.25$. When $k^2 < 0.5$ they are given by,

$$w = r^{1/4+\mu/2} \, (1-r)^{m/2} \, , \tag{22}$$

providing that $m + \mu = \frac{1}{2}$. When $k^2 > 0.5$ they are given by,

$$w = r^{1/4-\mu/2} \, (1-r)^{m/2} \, , \tag{23}$$

providing that $m - \mu = \frac{1}{2}$. These two solutions define the curve $J = k^2 \, (1 - k^2)$ that delimits in the $J - k$ plane the domain where Kelvin-Helmholtz instabilities exist (Drazin 1958, and thick dotted line in Fig. 4 here).

In the presence of a ground, the matching in Eq. 15 gives $R = A/B = 0$ when $\mathcal{R}e \to \infty$. In this case, the inviscid solution in BB67 (Eq. 6) reduces to $Bz^{1/2+\mu}$. Hence, as the asymptotic form of the neutral mode in Eq. 22 near $z = 0$ is of the same form, this neutral mode is also a solution (see the thick and solid line in Fig. 4). This is not the case for the solution in Eq. 23: its asymptotic form near $z = 0$ is $z^{1/2-\mu}$ and differs from the inviscid solution of BB67 with $A = 0$.

When $\delta \neq 0$ we can return to the analytical solution in the Eq. 18 and vary k to find if there are cases where both the matching conditions and the condition $|q| = |U_p/D_o| = \infty$ are satisfied. If we limit the investigation to real values for k this never occurs: one needs to consider that the inviscid solution above the boundary layer decay downstream, replacing k by $k + ik_i$ where k is still real while k_i is a positive constant characterizing the decay rate of the trapped solution. Providing that k_i is small (more specifically of the order of δ^β, where β is a positive constant) the inner set of equations in Section 3 remains the leading order approximation of our problem in the viscous layer. In this case, the results for $\tilde{R}$ in Fig. 2 and the matching in Eq. 15 remain appropriate, and we can use a complex wavenumber $k + ik_i$ to treat the inviscid problem in Eqs. 18–20.

The results for k when $\delta = 10^{-2}$ and $\delta = 10^{-4}$ are shown by the thick dashed lines in Fig. 4. They show that the introduction of a viscous boundary layer tends to increase the horizontal wavelength of the trapped solutions when compared to the inviscid solutions. Note also that the decay rate k_i (thick grey lines) also increases when the dissipation increases (note that in Fig. 4, the k_is are normalized by $\sqrt{\delta}$ for clarity). Finally, note also that the decay rate k_i increases when J increases, which is consistent with the fact that for a fixed viscous length δ, the gravity wave absorption by the boundary layer increases when J increases (Section 4.1).

5 Conclusion

The central motivation of this note are in the recent papers by Jiang et al. (2006) and Smith et al. (2006) which establish that the downstream development of trapped lee-waves is affected by the absorption of the stationary GWs by the boundary layer. They managed to quantify the downstream attenuation of mountain lee-waves, using a wave reflection factor by the boundary layer, q. They show that the downstream attenuation of trapped lee waves is controlled by this parameter, it is small when the amplitude of q is near 1, and it is large when the amplitude of q is small. Jiang et al. (2006) also made the point that the boundary layer can be a very effective absorber for the stationnary GWs, because the mean wind is very small near the ground, so the stationary GWs can have a critical level there. Smith et al. (2006) also proposed that the wave absorption by the boundary layer is related to the disturbance energy loss resulting from the fact that the disturbance in the boundary layer is shifted upstream when compared to the disturbance above it. This note analyzes these issues in the reference configuration where the critical level dynamics and the boundary layer dynamics are viscous.

First, we show on two examples, that in the viscous case the disturbance in the viscous layer is indeed in advance with the disturbance above it (see the phases in the right panels of the Figs. 1a, b). This result is consistent with the wave absorption mechanism proposed by Smith et al. (2006), and in which this phase shift is produced by the turbulent fluxes at the ground and at the top of the boundary layer.

A more precise evaluation of the boundary layer wave absorption is given in Fig. 2, which shows the fraction $\tilde{R}$ between the two viscous solutions that matches the inviscid solutions of BB67. This fraction combined with the matching condition in Eq. 15 are of a general interest: they permit to evaluate the fraction between the two inviscid solutions of BB67 without treating again the full viscous problem. They also give the main result of this note: there is always absorption by a viscous boundary layer, it can be very small when $J < 0.25$ and it increases with J when $J > 0.25$ (see Section 3).

As the results in section 3 are based on the analysis of of a boundary layer embedded within a background shear, the fraction R is not exactly measuring the fraction between an upward propagating wave and a downward propagating waves (this is particularly evident when $J < 0.25$, see Eq. 6). Hence, to measure precisely how the viscous layer reflects a stationary GW, we adopt in Section 4 the background flow profile in Eq. 1. For this profile, it is found that the reflection of a GW $|q| \approx 1$ when $J < 0.25$ and when the dissipation is small, as expected from the analysis in Section 3 (Fig. 3). When $J > 0.25$ it shows that $|q| < 1$, again as expected from Section 3, but it also shows substantial modulations of this coefficient which are related to the relative phase of the two inviscid solutions in BB67 at the top of the viscous layer. Nevertheless, the upper and lower bound for $|q|$ when this phase varies indicate that the dominant behavior is that the absorption increases ($|q|$ decreases) when J increases. This is also consistent with the findings by Jiang et al. (2006) who found that the more unstable boundary layers favor the onset of trapped lee waves.

Finally, and still for the profile in Eq. 1, we also found that when $J > 0.25$ the viscous boundary layer absorption is substantially smaller than that predicted by the full critical level interaction theory, and that it is also substantially smaller than that predicted using Rayleigh friction and Newtonian cooling (as done in Jiang et al. 2006).

To a certain extent the fact that the critical level dynamics in part control trapped lee-waves, suggests that there are some correspondences between trapped lee-waves and Kelvin-Helmholtz instabilities. After all, the idea that an almost total reflection should exist for trapped-lee

waves to develop, is quite near the idea that overreflection should exist for Kelvin-Helmholtz instabilities to exist (Lindzen and Rosenthal 1983). Not also that in our continuous context, the wave absorption mechanism proposed by Smith et al. (2006) also means that the boundary layer forces the disturbances near the ground to be tilted in the direction of the shear, which yields to disturbance energy loss according to the Orr mechanism (see Lott 1997 where this is analyzed in the context of GWs). According to Lindzen (1988), this transient Orr mechanism is also controlling the overreflection of GWs. The analogy is supported here, where it is shown that some among the neutral modes for Kelvin-Helmholtz instability can also be pure trapped waves when the Reynolds number is infinite (Fig. 4).

When the Reynolds number is finite, these trapped waves are modified, their amplitude decay downstream with a decay rate that increases when the dissipation increases and when the Richardson number increases. All those results are consistent with the picture that the decay rate should increase when the reflective factor q increases. Note that in the viscous case here, the dissipation also tends to increase the horizontal wavelength of the trapped solutions, which is the only result of this note which contradicts Smith et al. (2006).

It is quite clear that the problem analyzed here is rather peculiar in the context of the interaction between GWs and critical levels. The results obtained are nevertheless in good agreement with the present understanding of these interactions. At large Richardson number, it is generally admitted that the WKB approach applies, it predicts that the vertical group velocity of a GW tends toward zero when it approaches a critical level. The GW never arrives at the critical level and is ultimately absorbed. This picture applies here, since there is always absorption when $J > 0.25$ and this absorption can be very substantial when $J > 10$ (Figs. 1 and 2).

At Richardson number $J < 0.25$, the GW looses its propagating character as it approaches a critical level. It can then pass through it and interacts dynamically with it (see for instance Lindzen 1988). When the critical level is at the ground, it appears that this dynamical interaction cannot lead to overreflection because the GW is forced to stay on one side of the critical level. Nevertheless, the fact that the GW reaches its critical level means here that it reaches the ground: this is the mechanistic reason for which an almost perfect reflection occurs when $J < 0.25$ and when the Reynolds number is large.

6 Appendix

To evaluate q in the inviscid case without solving the viscous problem, it is conventional to introduce a small linear damping in the Eq. 2 (see again BB67 where this approach is presented). In this case, the solution in Eq. 6 transforms into:

$$w \approx A\left(z - \frac{i\alpha}{k}\right)^{1/2+i\mu} + B\left(z - \frac{i\alpha}{k}\right)^{1/2-i\mu}, \tag{24}$$

where α is a positive constant representing Newtonian cooling and Rayleigh friction. In $z = 0$, the boundary condition $w = 0$ implies:

$$q = -\left(-\frac{i\alpha}{k}\right)^{-2i\mu}. \tag{25}$$

In the limit $\alpha \to 0$, this yields to

$$|q| = 0 \text{ when } J < 0.25 \text{ and } |q| = e^{-\mu\pi} \text{ when } J > 0.25. \tag{26}$$

The null value for $J < 0.25$ is like in the inviscid limit in Section 3, while the decay when J increases beyond 0.25 is much faster than in inviscid limit (not shown but when $J > 0.25$ $|q| = |\tilde{R}|$, so the viscous values of $|q|$ are also in Fig. 2)

As in Section 4, q can be translated in the reflection of a GW coming from $z = \infty$. This yields to $|R| \approx 1$ when $J < 0.25$, as in the viscous case, and $|R| < 1$ when $J > 0.25$, with a decay when J increases more pronounced than in the viscous case. In particular, when $J > 1$, $|R|$ becomes very near the reflection coefficient predicted by the full critical level interaction theory (see VK82).

Acknowledgments

The comments of two anonymous reviewers were very helpful in clarifying this note.

References

Baldwin, P. and P. H. Roberts, 1970: The critical layer in stratified shear flow, *Mathematika*, **17**, 102–119.

Brankin, R.W., I. Gladwell, and L.F. Shampine, 1991: A suite of Runge-Kutta codes for the initial value problems for ODEs, *Soft Report 91-1, Math. Dept.*, Southern Methodist University, Dallas, Texas.

Booker, J. R. and F. P. Bretherton, 1967: The critical layer for internal gravity waves in a shear flow, *J. Fluid Mech.*, **27**, 513–539.

Bougeault, P. and Coauthors, 1993: The atmospheric momentum budget over a major mountain range: first results of the PYREX experiment, *Ann. Geophys.,* **11,** 395–418.

Bougeault, P. and Coauthors, 2001: The MAP special observing period, *Bull. Amer. Meteor. Soc.,* **82,** 433–462.

Bougeault, P. and P. Lacarrere, 1989: Parameterization of orographic induced turbulence in a mesobeta scale model, *Month. Weath. Rev.*, 117, 1872–1890.

Drazin, P. G., 1958: The stability of a shear layer in an unbounded heterogeneous inviscid fluid, *J. Fluid Mech.*, **4,** 214–224.

Georgelin, M., E. Richard, M. Petitdidier, and A. Druilhet, 1994: Impact of subgrid-scale orography parameterization on the simulation of orographic flows, *Month. Weath. Rev.*, **122**, 1509–1522.

Hazel, P., 1967: The effect of viscosity and heat conduction on internal gravity waves at a critical level, *J. Fluid Mech.*, **30**, 775–783.

Jiang, Q., J. D. Doyle and R. B. Smith, 2006: Interaction between trapped waves and boundary layers, *J. Atmos. Sci.*, **63**, 617–633.

Lindzen, R. S., 1988: Instability of plane parallel shear flow (toward a mechanistic picture of how it works), *Pageoph*, **126**, 103–121.

Lott, F., 1997: The transient emission of propagating gravity waves by a stably stratified shear layer, *Quart. J. Roy. Meteor. Soc.*, **123**, 1603–1619.

Lott, F., H. Kelder, and H. Teitelbaum, 1992: A transition from Kelvin-Helmholtz instabilities to propagating wave instabilities, *Physics of Fluids A*, **4**(9), 1990-1997.

Lott, F., and H. Teitelbaum, 1992: Nonlinear dissipative critical level interaction in a stratified shear flow: instabilities and gravity waves,*Geoph. and Astroph. Fluid Dyn.*, **66**, 133–167.

Oberhettinger, F. 1970: Hypergeometric functions, *Handbook of Mathematical functions,Edited by M. Abramowitz and I. A. Stegun*, Dover Publications, Inc., New-York, 555–566.

Richard, E., P. Mascart and E. C. Nickerson, 1989: The role of surface friction in downslope windstorms, *J. Appl. Meteor.*, **28**, 241–251.

Rosenthal, A. J., and R. Lindzen, 1983: Instabilities in a stratified fluid having one critical level. Part III: Kelvin-Helmholtz instabilities as overreflected waves, *J. Atmos. Sci.*, **40,** 530-542.

Scorer, R. S., 1949: Theory of waves in the lee of mountains, *Quart. J. Roy. Meteor. Soc.*, **75**, 41–56.

Smith, R. B., Q. Jiang and J. D. Doyle, 2006: A theory of gravity wave absorption by a boundary layer, *J. Atmos. Sci.*, **63**, 774–781.

Smith, R. B., S. Skubis, J. D. Doyle, A. S. Broad, C. Kiemle, and H. Volkert, 2002: Mountain waves over the Mont Blanc: Influence of a stagnant boundary layer, *J. Atmos. Sci.*, **59**, 2073–2092.

Van Duin, C. A. and H. Kelder, 1982: Reflection properties of internal gravity waves incident upon an hyperbolic tangent shear layer, *J. Fluid. Mech.*, **120**, 505–521.

Van Duin, C. A. and H. Kelder, 1986: Internal gravity waves in shear flows at large Reynolds number, *J. Fluid Mech.*, **169**, 293–306.

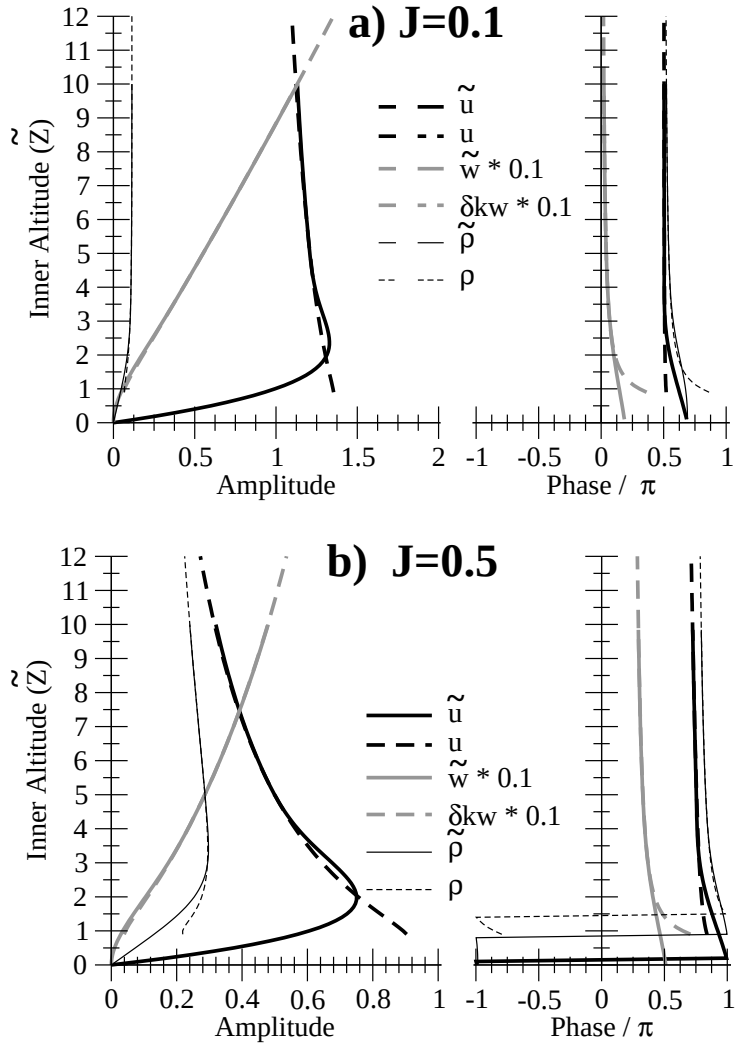

Figure 1: Outer and inner solutions expressed with the inner variables in Eq. 10 and for $\mathcal{P}r = 2$, $k = 0.1$, and $\delta = 10^{-2}$ ($\mathcal{R}e = 10^7$): a) $J = 0.1$ and b) $J = 0.5$. $\tilde{u}$ (thick solid) ,$\tilde{w}$ (thick grey solid), and $\tilde{\rho}$ (thin solid) are from the Runge-Kutta numerical integration of the viscous Eq. 11; u (thick dashed), $w/(\delta k)$ (thick grey dashed), and ρ (thin dashed) are from the inviscid solution of BB67 in Eq. 6. Note that $\tilde{w}$ and $w/(\delta k)$ have been multiplied by 0.1 for clarity.

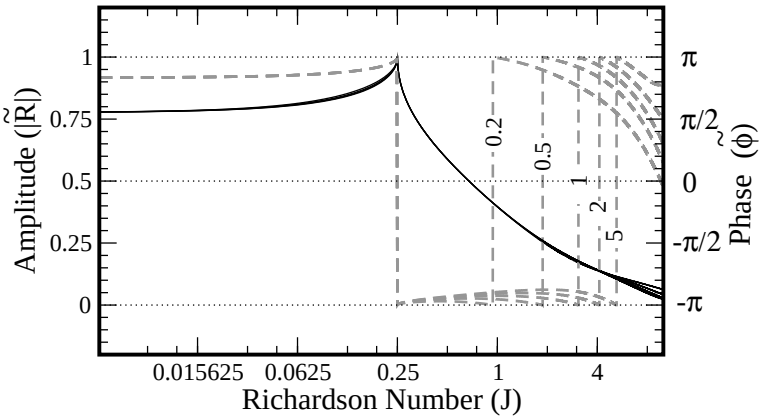

Figure 2: Ratio $\tilde{R}$ (Eq. 15) between the viscous solutions that match the inviscid solutions of BB67 and for five different values of the Prandtl number: $\mathcal{P}_r = 0.2, 0.5, 1, 2, 5$. Amplitude $|\tilde{R}|$ (thin solid), phase $\tilde{\phi}$ (thick grey dashed). Note that the horizontal axis is in logarithm.

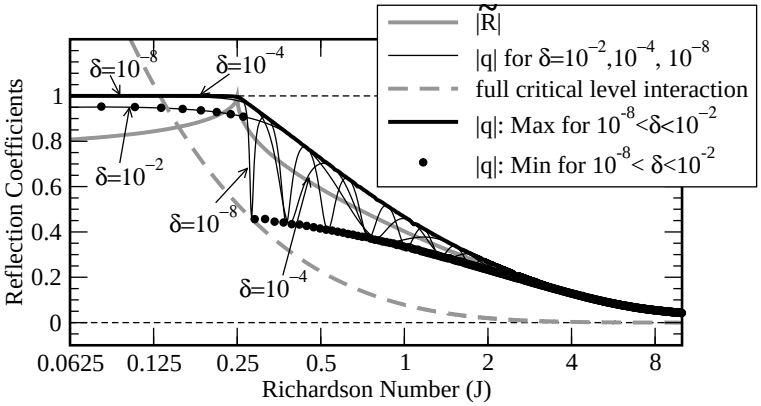

Figure 3: Boundary layer reflection of a GW coming from $z = \infty$ and for the full tanh flow profile in Eqs. 1, $\mathcal{P}r = 2$, and $k = 0.1$: $|q|$ for three values of δ (thin solid), Maximum and Minimum of $|q|$ when δ varies between 10^{-8} and 10^{-2} (or when the Reynolds number $\mathcal{R}e$ varies between 10^7 and 10^{25}, thick black solid and thick black dots respectively), inner fraction $|\tilde{R}|$ (thick grey), and $|q|$ for a full critical level interaction (thick grey dashed) (inviscid values from VK82). Note that the horizontal axis is in logarithm.

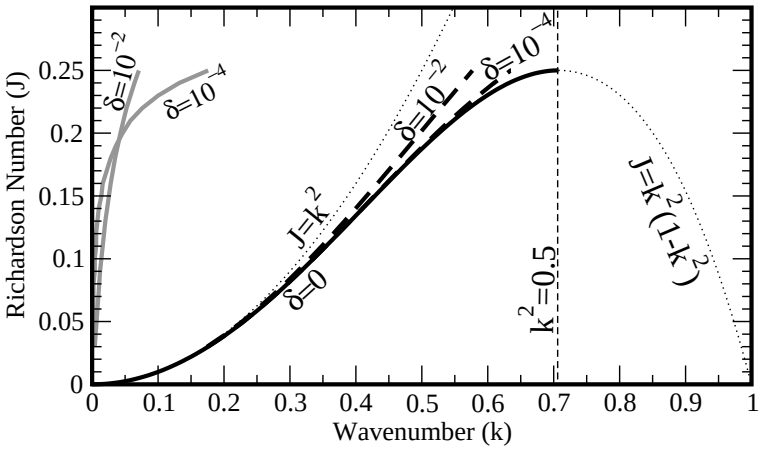

Figure 4: Horizontal wavenumber of the trapped solutions that exist in the mean flow profile in Eq. 1: k for $\delta = 0$ (thick solid); k and $k_i/\sqrt{\delta}$ for $\delta \neq 0$ (thick dashed and thick grey respectively). The dotted lines also show: the limit curve for Kelvin-Helmholtz instabilities, $J = k^2(1 - k^2)$; and the limit curve for GW propagation in $z = \infty$, $J = k^2$.